Nanoimprint lithography with ≤60 nm overlay precision

Wei Wu · Robert G. Walmsley · Wen-Di Li · Xuema Li ·
R. Stanley Williams

Abstract Nanoimprint lithography is a high-resolution, high-throughput and cost-effective nanopatterning technology. However, the overlay accuracy is lagging behind the resolution because of the high cost of mechanical precision. We have built an inexpensive stand-alone machine based on the wafer bowing nanoimprint process, and demonstrated single-point overlay of two transferred pattern layers with an accuracy of ≤60 nm.

1 Introduction

Nanoimprint lithography (NIL) [1] is a high-resolution, high-throughput and cost-effective nanopatterning technology based on mechanical deformation of the resist instead of chemical modification of the resist by radiation. In photolithography, the light not only transfers the pattern information, but also works as a low-pass spatial information filter, which limits resolution (i.e. diffraction limit). In NIL, the pattern information is transferred directly by a mechanical deformation or imprint process that is not limited by optical resolution and, therefore, NIL provides much higher resolution potential. For example, we have demonstrated isolated lines down to 5 nm and dense lines with half-pitch down to 12 nm [2]. However, the mechanical transfer process also provides a new set of challenges, most notably the problem

of overlay; that is, the alignment to previous patterns and the maintenance of that alignment as the mold approaches and contacts the substrate. Overlay accuracy approaching resolution limits demands exceptionally precise mechanical movement, and commensurate mechanical and thermal stability. The highly sophisticated mechanical precision required to meet these demands implies substantial cost [3, 4], but overlay accuracy better than 20 nm has been achieved in commercial systems [5]. While such nanoimprint machines are less expensive than state-of-the-art photolithography or extreme UV lithography (EUVL) machines, they are intended for production use and may be out of reach of a typical research budget. We have constructed a lower-cost alternative based on wafer bowing (Fig. 1). In this approach, the mold is brought into contact with the substrate by means of a process that is local to the mask and wafer. There is no external machine movement, and alignment is maintained by direct contact between mask standoff features on the wafer. Differential gas pressure is used to deform or bow the wafer, bringing it into contact with the patterned area of the mask plate. To demonstrate this principle, we previously built a simple nanoimprint module, which can be added to a contact photolithography mask aligner to transform it into a UV nanoimprint machine, and demonstrated an overlay accuracy of <0.5 μm and a resolution of <10 nm [2]. The overlay accuracy was mainly limited by the mechanical instability of the mask aligner and the resolution of the optical microscope. In order to realize the potential of the wafer bowing NIL process, we purpose built a stand-alone UV nanoimprint machine with four major improvements. First, we used a cascaded mechanical design that allowed transfer of mask-to-wafer position control from an external positioning system within the imprint module to one internal to the mask and wafer. Second, we built the machine on a platform more stable than a typical contact mask aligner. Third,

W. Wu (✉) · R.G. Walmsley · W.-D. Li · X. Li · R.S. Williams
HP Labs, Hewlett-Packard Co., Palo Alto, CA 94304, USA
e-mail: wu.w@usc.edu

R.G. Walmsley
e-mail: bob.walmsley@hp.com

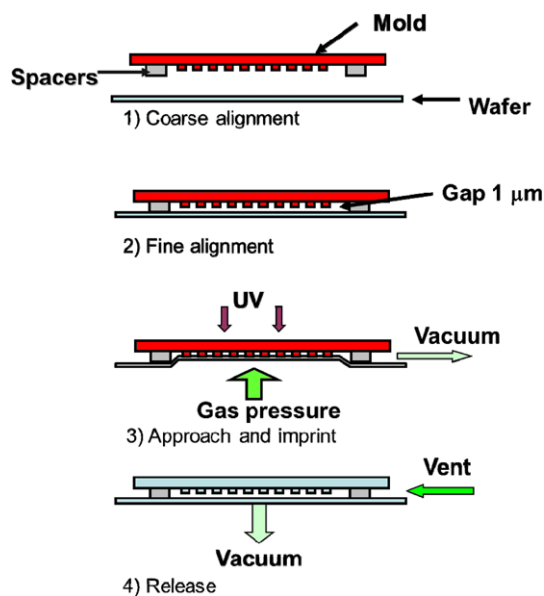R.S. Williams
e-mail: stan.williams@hp.com

Fig. 1 Schematic of nanoimprint process using wafer bowing

we implemented fully automated gas pressure control, allowing vacuum/pressure and pneumatic sequences to be entirely computer controlled. That gave us precise control of both the wafer bowing and the load applied by the mold. Fourth, an $x-y$ closed-loop piezo stage was added in order to perform the nanoalignment. With this NIL machine, we achieved ≤ 60 nm overlay accuracy by using Moiré patterns as alignment markers. With design changes that would include $x-y$ and rotational direct nanoalignment of the mold together with temperature control to within $0.1°C$, $\sim$10-nm alignment over a 25-mm field should be possible with this system.

2 Machine description

The nanoimprint machine (Fig. 2) consists of three subsystems, the imprint module, the pneumatic control and the imaging system. The machine is built on a granite table that is similar to those used for an atomic force microscope (AFM). The table sits on four air mount vibration isolators (I-200 series, Newport Co., Irvine, CA) to isolate the vibrations from the floor. A vertical granite block is mounted on the granite base to mount the camera system.

The imprint module (Fig. 3) is the key component of the machine, where both the final alignment and imprint occur. The center piece of the module is a wafer support, which is essentially the same as the nanoimprint chuck we reported previously [2], except that it is made of super-invar for thermal stability. The wafer chuck is divided into two zones, inner and outer, by a hollow O-ring. There is also an inflatable O-ring close to the perimeter of the chuck. The chuck is mounted on top of a piezo $x-y$ nanomover (N-XY100A-1,
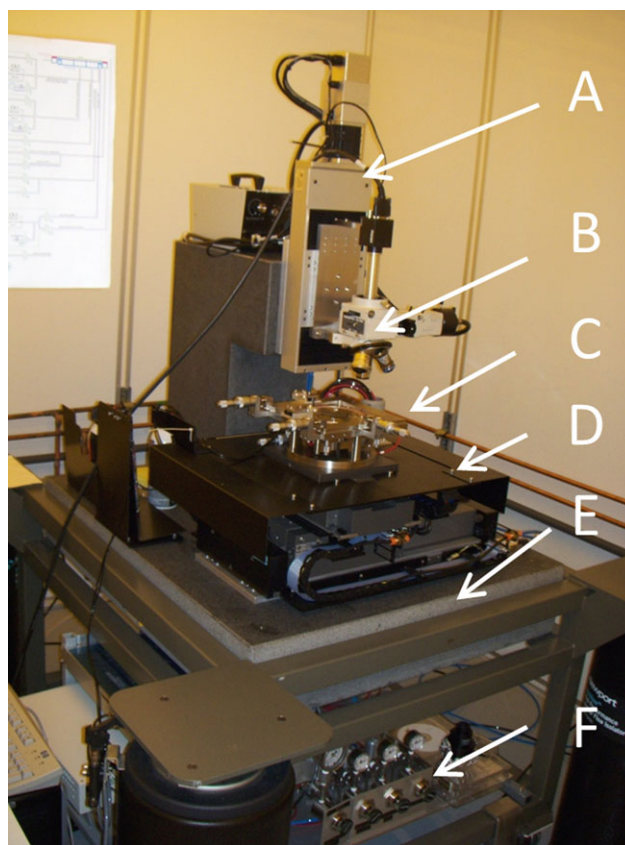

Fig. 2 A picture of the nanoimprint machine. *A* linear mover for '*z*', *B* microscope, *C* nanoimprint module, *D* '*x*−*y*' stage, *E* granite table, *F* pneumatic controls

nPoint Inc., Middleton, WI), which has $\sim$1-nm resolution. The nanomover is mounted on a frame also constructed of super-invar. On top of the wafer chuck is the mold locator within which the mold is kinematically located in x and y axes by a controlled preload. The mold locator magnetically couples to three micrometers mounted on the imprint module frame. These three frame micrometers allow coarse $x-y$ and rotational alignment of the mold locator relative to the frame by means of an air bearing. Once coarse alignment is achieved, the air bearing is landed (vacuum locked) and the micrometers disengaged, thus fixing the mold locator to the frame. There are also four vertical micrometers, which sit at the four corners of the mold, to adjust the gap between the mold and the wafer during coarse alignment. The frame sits on top of a rotation stage, which is used to align the wafer coordinate frame to the microscope stage coordinate frame. The rotation stage is also an air bearing that is vacuum locked after alignment.

The imaging sub-system consists of a mono-color digital camera (AccuPixel, JAI Ltd., Japan), a motorized $x-y$ air-bearing stage (Aero Tech ES15844-1, RCS Rocket Motor Components Inc., Cedar City, UT) and a motorized linear z stage. The camera is mounted on the linear z stage, which
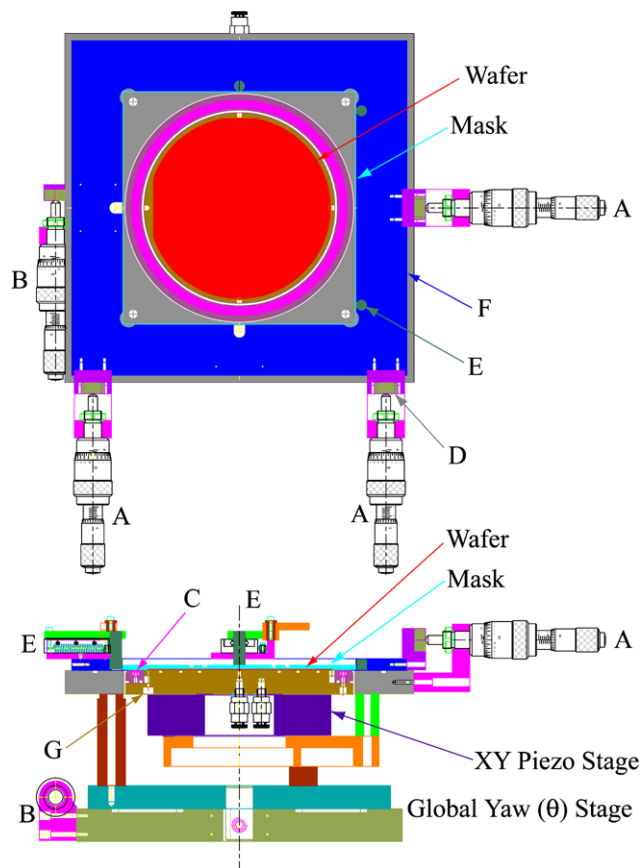
Fig. 3 A mechanical drawing of the imprint module. *A* micrometer for *x−y* and *θ*, *B* micrometer for global yaw adjustment, *C* inflatable O-ring, *D* coupling magnet, *E* mask contacts, *F* mask holder, *G* wafer holder

in turn is mounted on the vertical granite block. The linear stage moves up and down ('*z*' direction) to enable camera focus. The *x−y* stage moves the imprint module laterally to position the camera over the mold/wafer alignment marks. The resolution of these stages is ∼100 nm in *z* and ∼10 nm in *x* and *y*. These stages are only responsible for optically accessing alignment marks; they do not directly control the mold-to-wafer alignment. Both stages are controlled though a nanoimprint computer program.

The pneumatic control system includes an array of valves and regulators providing the necessary pressures. In addition, three computer-interfaced controllers (640A, MKS Instruments, Andover, MA) determine the pressure under the wafer, above the wafer and inside the inflatable O-ring. All the valves and pressure controllers are under programmatic control.

There are no 'brute force' high-precision mechanical couplings in this machine, and all the components are either standard off-the-shelf parts or parts that can be made by a standard machine shop. These considerations make this machine a cost-effective solution for nanopatterning with high-precision overlay.

3 Operational procedure and experimental results

In order to demonstrate the machine, we patterned two sequential metal layers, first Au and then Pt, by UV NIL and metal lift-off. The mold substrates were 5-in. quartz photomask plates with a 60-nm SiN_x film deposited by PECVD. Ti spacers with a height of 1 μm were deposited outside the imprint field. Patterns on those molds were etched into the SiN_x layer with a feature height of 60 nm. This machine was designed to imprint on 4-in. wafers, but it can be used to pattern substrates with other sizes by using chucks with different form factors. A double-layer UV-curable NIL resist [6, 7] with 60-nm transfer layer and 75-nm liquid imaging layer was used.

The nanoimprint process for each layer was divided into the following steps: (1) coarse alignment, (2) fine alignment, (3) approach and imprint and (4) release (Fig. 1). First, a wafer was loaded onto the wafer chuck, and a mold into the mold locator on top of the wafer. The gap between the mold and substrate was set by the four vertical micrometers. The wafer coordinate frame was then aligned to the optical system coordinate frame by rotation of the imprint module. Next, a coarse alignment of the mold pattern to the wafer in *x−y* and rotation of ±1 μm and 10 μrad, respectively, was performed by adjusting the three frame micrometers. After the coarse alignment, the mold, or more specifically the spacers on the mold, was landed onto the substrate by lowering the four vertical micrometers, and the air bearing of the mold locator was switched to vacuum to lock it. The lockdown bypassed the moving mechanism for the coarse alignment and shortened and stiffened the mechanical path between the mold and wafer, reducing differential movement between the mold and substrate. At this point, a small load was applied between the mold and wafer by pressurizing the inflatable O-ring to seal the mold to the wafer support and then drawing a small vacuum (∼30 Torr below atmosphere) in the gap between the mold and substrate. The resultant preload ensured intimate spacer-to-wafer contact while minimizing in-plane friction, and it brought the mold and wafer contact surfaces within the focus depth of the optics.

At this stage, the piezo nanomover was used to translate the wafer relative to the mold for single-point *x−y* alignment. In order to achieve an alignment accuracy better than the resolution of the optical microscope, Moiré fringe alignment markers [8–10] were used. Two sets of Moiré fringes were used for both *x* and *y* directions (Fig. 4). In one set, a 1.2 μm pitch grating was in the first layer and a 1.22 μm pitch grating in the second layer; in the other set, the 1.22 μm pitch grating was in the first layer and the 1.2 μm pitch grating in the second layer. The distance between two fringes '*d*' is a function of the misalignment 'Δl':

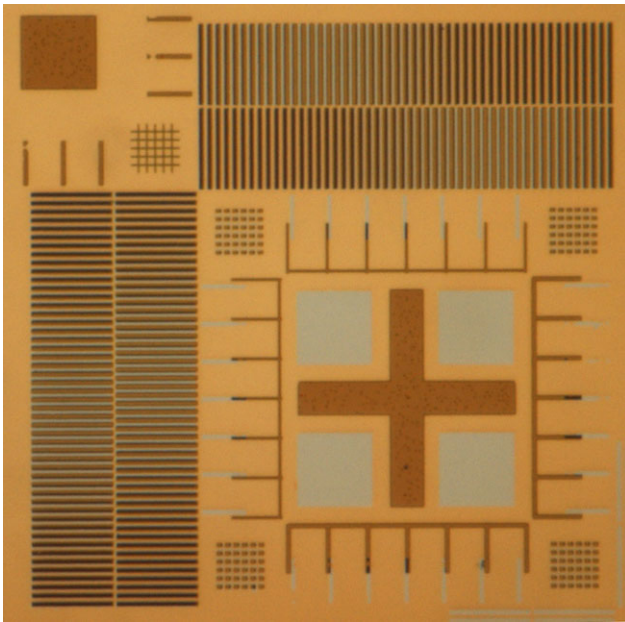$$d = \frac{p_1 + p_2}{p_1 - p_2} \Delta l,$$

Fig. 4 An optical image of the alignment markers. The *dark patterns* were from the first nanoimprinted layer and the *bright patterns* were from the second nanoimprinted layer. Both vernier and Moiré patterns are shown in the picture

where 'p_1' and 'p_2' are the pitches of the two gratings. For this configuration, the misalignment was magnified by a factor of 120. For example, a 10-nm misalignment (Δl) between the two layers would result in a 1.2-μm misalignment (d) in the Moiré fringes. After fine alignment, the center zone of the wafer support was ramped to atmospheric pressure, and the gap between the wafer and mold was pumped to a pressure of <40 Torr. As a result of this pressure difference, the wafer bowed up and the mold bowed down to press the patterns on the mold into the imaging layer of the resist. After the resist was cured by UV light, the gap was vented to atmosphere and the inner zone of the wafer chuck was pumped to vacuum. By raising the four vertical micrometers, the mold and substrate were separated.

Figure 5 shows an overlay of two metal layers. The Au metal box array was the first layer and the Pt grid was the second layer. The zoomed-in image shows an overlay accuracy of ≤60 nm. For a more precise measurement of the overlay, we compared the center location of each of the 4×4 box and frame pairs using purpose-written software. The overlay errors were 59.0 ± 2.2 nm in the 'x' direction and 1.4 ± 1.9 nm in the 'y' direction. The master NIL mold was fabricated by electron-beam lithography (EBL) using a scanning electron microscope (SEM, FEI) with a pattern generator; this system has a small pattern distortion within the writing field, which was the main reason for the variations in the overlay.

4 Discussion

The overlay errors were mainly due to the 'slip and stick' between the mold and substrate during the fine alignment. Ideally, the 1-μm gap between the wafer and mold surfaces is formed by the landing spacers on the substrate, where all spacers are in contact with the substrate surface at the same time with little vertical load. If the friction is small enough, the spacers should slide on the wafer surface smoothly. However, in reality, none of the mold, substrate or chuck surfaces is perfectly flat. Therefore, the mold and substrate need to be under enough pressure to make the spacers form a good contact with the substrate in order to form a small gap for high-contrast Moiré fringes. However, this pressure increases the friction to the point that the nanomover cannot move smoothly, but rather the wafer and mold translate relative to each other by slip and stick motion. Usually, the nanomover did not translate if we commanded it to move a short distance (≤100 nm), but it would suddenly jump if we kept increasing the distance. Thus, even though our Moiré pattern alignment markers are capable of ∼10-nm alignment in theory, we could only realize 60-nm overlay accuracy in the 'x' direction. With 'better luck', we had an almost perfect alignment in the 'y' direction.

Currently, this machine is only capable of single-point fine alignment, which is actually satisfactory for many research applications. In order to achieve global fine alignment, two issues must be addressed: the existing x–y piezo nanomover is not capable of rotational motion, and there is no temperature control implemented in the machine. We plan to replace the x–y nanomover with three linear piezo nanomovers providing three-degrees-of-freedom fine movement of the mold rather than the substrate support. Moreover, linear nanomovers have a much larger load capacity than compact 'x–y' nanomovers, so they should overcome the stiction of the contact pads and improve the alignment accuracy as well. With a differential thermal expansion coefficient of 2.4×10^{-6}/°C between the Si wafer and quartz mold and an imprint field of 1 in., 1°C of temperature difference across an imprint field creates a 60-nm alignment difference from edge to edge. Thus, ∼0.1°C temperature control will be necessary to achieve sub-10-nm global alignment. However, this temperature-controlled environment need only surround the imprint module, maintaining the wafer and mold within 0.1°C of a reference temperature, for example the standard metrology temperature of 21°C.

The slip distance of the nanomover is due to the stiction between the spacers and substrate, and the larger the stiction, the larger the slip distance. The stiction comes from the pressure load needed to maintain the gap between the substrate and mold to generate Moiré fringes. Therefore, it is critical to maintain the gap with the lowest pressure. A 4-in. Si wafer has a thickness of 0.5 mm and the mold

Fig. 5 SEM images of two metal layers fabricated by NIL and metal lift-off. The box array was patterned first and the mesh second. The box was made of Au and the mesh was made of Pt. The *bottom image* shows an overlay accuracy of about 60 nm
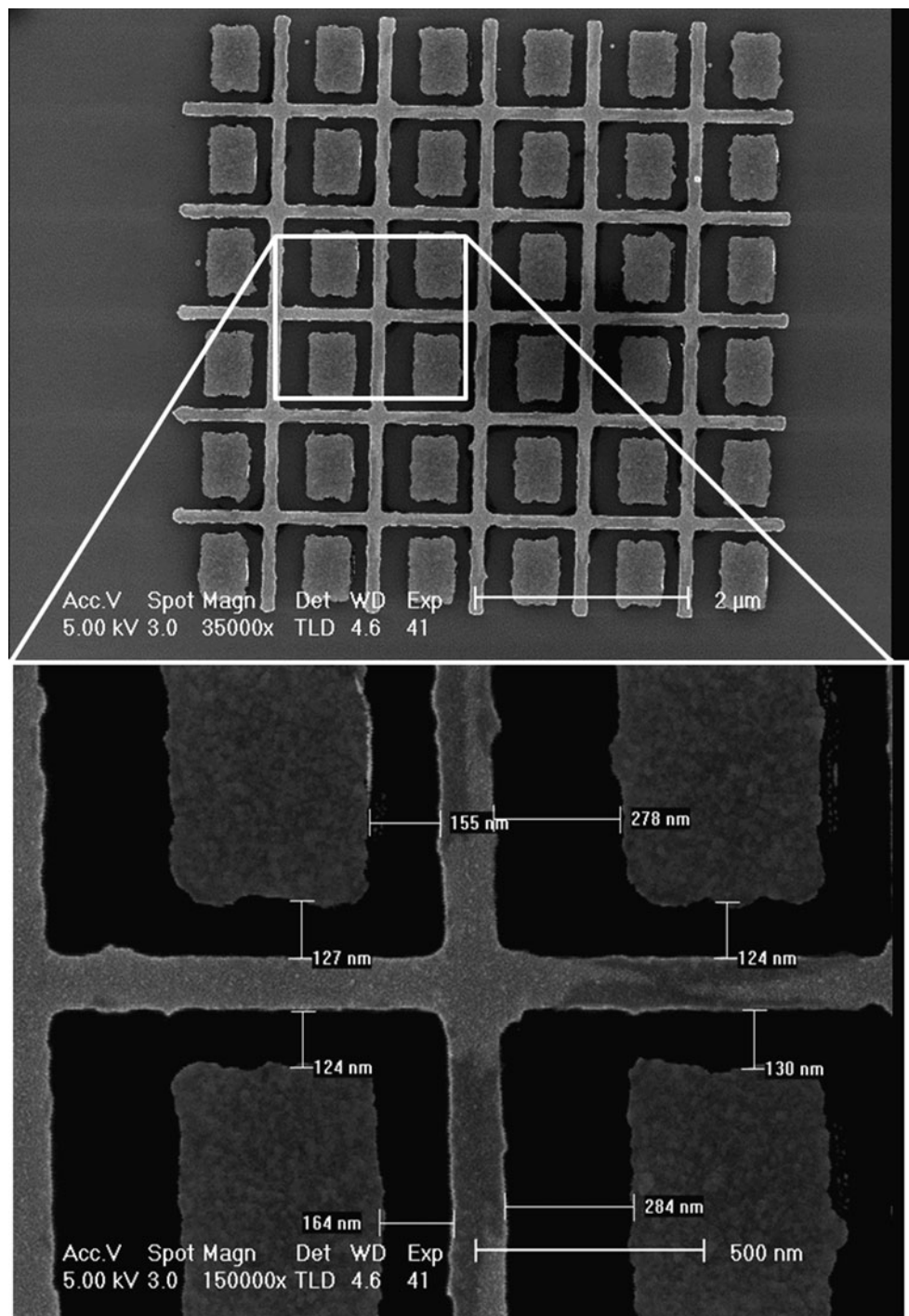
substrate is a 2.4-mm-thick quartz plate; hence, the substrate side is much more flexible, and it is more effective to deform the substrate side to reach the small gap needed for the Moiré fringes. To implement this, we lowered the gap pressure to 730 Torr (i.e. 30 Torr below atmosphere) first and then ramped up the pressure in the inner zone of the wafer chuck until Moiré fringes appeared. If the gap was too large to have clear Moiré fringes, we ramped the pressure in the

gap down until the fringes appeared. If we kept the inner zone of the wafer support at vacuum, it would have required a much larger load on the mask to have good Moiré fringes.

5 Summary

We implemented the wafer-bowing NIL process with a cost-effective stand-alone nanoimprint machine using read-

ily available components and parts made by a standard machine shop. Using this machine, we demonstrated single-point overlay of two transferred pattern layers with an accuracy of ≤60 nm. By replacing the compact '$x-y$' piezo mover with three linear piezo movers together with temperature control to within 0.1°C, ~10-nm overlay over a 25-mm field should be possible.

References

1. S.Y. Chou, P.R. Krauss, P.J. Renstrom, J. Vac. Sci. Technol. B **14**(6), 4129–4133 (1996)
2. W. Wu, W.M. Tong, J. Bartman, Y.F. Chen, R. Walmsley, Z.N. Yu, Q.F. Xia, I. Park, C. Picciotto, J. Gao, S.Y. Wang, D. Morecroft, J. Yang, K.K. Berggren, R.S. Williams, Nano Lett. **8**(11), 3865–3869 (2008)
3. Z.M. Ye, R. Ramos, C. Brooks, L. Simpson, J. Fretwell, S. Carden, P. Hellebrekers, D. LaBrake, D.J. Resnick, S.V. Sreenivasan, in *Alternative Lithographic Technologies III*, ed. by D.J.C. Herr. SPIE Proc., vol. 7970 (SPIE Press, Bellingham, 2011)
4. L. Singh, K. Luo, Z.M. Ye, F. Xu, G. Haase, D. Curran, D. LaBrake, D. Resnick, S.V. Sreenivasan, in *Alternative Lithographic Technologies III*, ed. by D.J.C. Herr. SPIE Proc., vol. 7970 (SPIE Press, Bellingham, 2011)
5. M. Malloy, L.C. Litt, Proc. SPIE **7637**, 763706 (2010)
6. W. Wu, G.-Y. Jung, D.L. Olynick, J. Straznicky, Z. Li, X. Li, D.A.A. Ohlberg, Y. Chen, S.-Y. Wang, J.A. Liddle, W.M. Tong, R.S. Williams, Appl. Phys. A **80**(6), 1173–1178 (2005)
7. M.D. Austin, H.X. Ge, W. Wu, M.T. Li, Z.N. Yu, D. Wasserman, S.A. Lyon, S.Y. Chou, Appl. Phys. Lett. **84**(26), 5299–5301 (2004)
8. S.R.J. Brueck, S.H. Zaidi, U.S. Patent, 5,216,257, 1993
9. M. Mühlberger, I. Bergmair, W. Schwinger, M. Gmainer, R. Schöftner, T. Glinsner, C. Hasenfuß, K. Hingerl, M. Vogler, H. Schmidt, E.B. Kley, Microelectron. Eng. **84**(5–8), 925–927 (2007)
10. N.H. Li, W. Wu, S.Y. Chou, Nano Lett. **6**(11), 2626–2629 (2006)